Relationship between melting and amorphization of ice

Osamu Mishima

National Institute for Research in Inorganic Materials, 1-1, Namiki, Tsukuba, Ibaraki 305, Japan

THE discovery[1] in 1984 that an ice crystal can be transformed by pressure to an amorphous phase has since been followed by other examples of pressure-induced amorphization[2]. This transition, like melting, involves loss of long-ranged order, prompting the question of whether the two transitions are related. Here I describe experiments probing this relationship for a form of crystalline ice (denoted Ih) which is melted and amorphized by pressure. To avoid the complication of crystal–crystal transformations interrupting the melting process I use an ice emulsion, in which the very small particle size (about 5 μm) suppresses nucleation of other crystal phases. As the temperature is decreased, I see a smooth crossover from (pressure-induced) equilibrium melting to sluggish amorphization at around 140–165 K. In this temperature range, ice Ih became 'supercompressed' before melting to a highly viscous liquid which seemed to be related to an imperfectly relaxed amorphous ice. Below about 140 K, ice Ih was transformed to an unrelaxed phase apparently related to the high-density amorphous form of ice. This sequence of transitions can be viewed as a crossover from a two-phase melting process (which is determined by the relative free energies of the solid and liquid phases) towards a one-phase amorphization process (where the transition is induced by a mechanical instability limit of the solid).

Between 273 and 250 K, ice Ih can be melted by applying pressure. When compressed at 77 K, ice Ih is amorphized[1]. But the relationship between these two transitions is hard to probe because, below about 250 K, ice Ih is transformed under pressure to other crystalline forms (such as ice III and IX) before melting occurs. Molecular-dynamics calculations[3,4] have provided some information on the relation between melting and amorphization, but experimental data are almost non-existent.

If the formation of these other crystal phases can be suppressed, however, ice Ih melts to metastable (supercooled) water below ∼250 K. By conducting pressurization experiments on ice Ih in an emulsion (see Fig. 1 legend), I have mapped out the melting and amorphization curves between 250 and 77 K (Figs 1, 2). This can be divided into four regimes.

In region A ($250\,K > T > 190\,K$), ice Ih undergoes thermodynamic (metastable) melting to supercooled water (in situ X-ray characterization of the liquid phase would be desirable, but has not yet been obtained). The transition pressures extrapolate smoothly to the bulk melting line above ∼250 K. The transition is endothermic (Fig. 3), and the transformed phase (supercooled emulsified water) could be recovered by decompressing to atmospheric pressure above 235 K. As the ice is compressed (quasi) adiabatically through the transition, the endothermic nature means that heat is absorbed by the melted fraction, the sample temperature decreases, and a higher pressure is needed to allow the transition to go to completion along the melting line of ice Ih. This shows that the melting is an equilibrium transition. I also observed melting of emulsified ice III, V and VI along their extrapolated melting lines, showing that this ability of emulsions to reveal metastable melting is quite general.

The crossover from region A to region B corresponds to the point at which other crystal phases can nucleate homogeneously in the supercooled water emulsion formed by melting of ice Ih. This homogeneous nucleation temperature of ∼190 K at 0.5 GPa was estimated by extrapolating that measured between 0 and 0.3 GPa (ref. 5). So in region B, the ice Ih emulsions were observed to transform to ice V between 190 and 180 K, and to ice IX or III

below ∼180 K. The latter occurred in two steps as the pressure was increased: gradually at first (a in Fig. 1, hatched area in Fig. 2a) and then quickly (b in Fig. 1, circles in Fig. 2a). The comparable sharpness of curve b in region B with melting at 197 K in region A (Fig. 1) suggests that the transitions in both regions A and B begin by the same mechanism, that is, melting of ice Ih. Moreover, the transitions at b extrapolate smoothly to the melting line in region A, and so it seems reasonable to regard them as the locus of a melting transition of ice Ih to supercooled water followed by freezing to ice V or IX. The transitions in region B are exothermic, consistent with the evolution of heat due to the net crystal–crystal (ice Ih to ice V or IX) transformation.
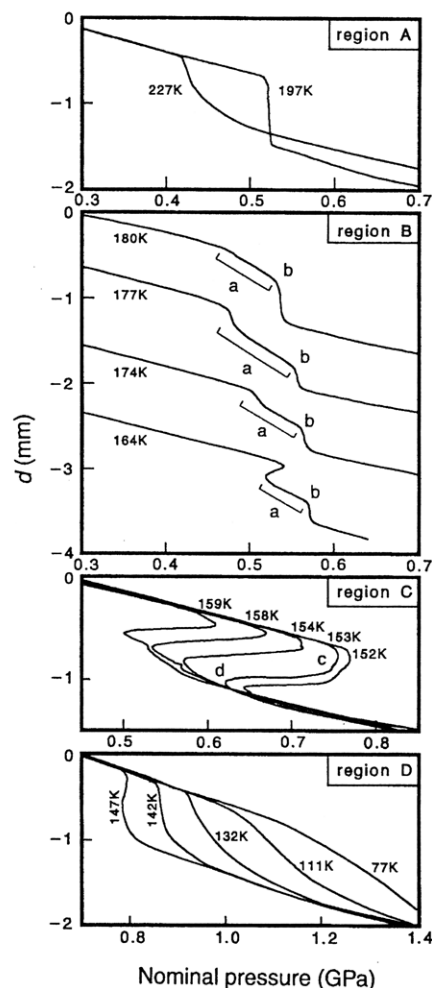

FIG. 1 Compression of fresh ice Ih emulsions (in terms of piston displacement d; see below) as a function of nominal pressure for first-compression runs. The temperature around the onset of transition is indicated. Volume of ice Ih decreased by ∼20% at the transitions in regions B, C and D, which agreed approximately with the change to ice V, IX or HDA. Compression of the emulsion carrier material between 77–273 K showed a monotonous decrease in volume.
METHODS. About 1.3 g of water emulsion[5] (droplets 1–10 μm in size), made by stirring methylcyclohexane (3 cm³), methylcyclopentane (3 cm³), distilled water (4 cm³) and sorbitan tristerate (200 mg) with a homogenizer, was loaded into an indium cup and compressed in a steel cylinder (bore diameter, 15 mm) by a hydraulic press[9]. The apparatus, cooled in a pail filled with liquid nitrogen, warmed gradually (∼1.3 K min⁻¹ at 100–150 K, ∼0.9 K min⁻¹ at 150–200 K) after the nitrogen evaporated. During the heating, the sample was compressed up to ∼1.5 GPa at a constant rate of 0.1 GPa min⁻¹ (except at transitions). The piston displacement (d), the press load and cylinder temperature were measured during the experiment. The given temperatures at high pressure are the cylinder temperatures and have an error of ± ∼3 K. The pressure of the sample is ∼90% of the nominal pressure.
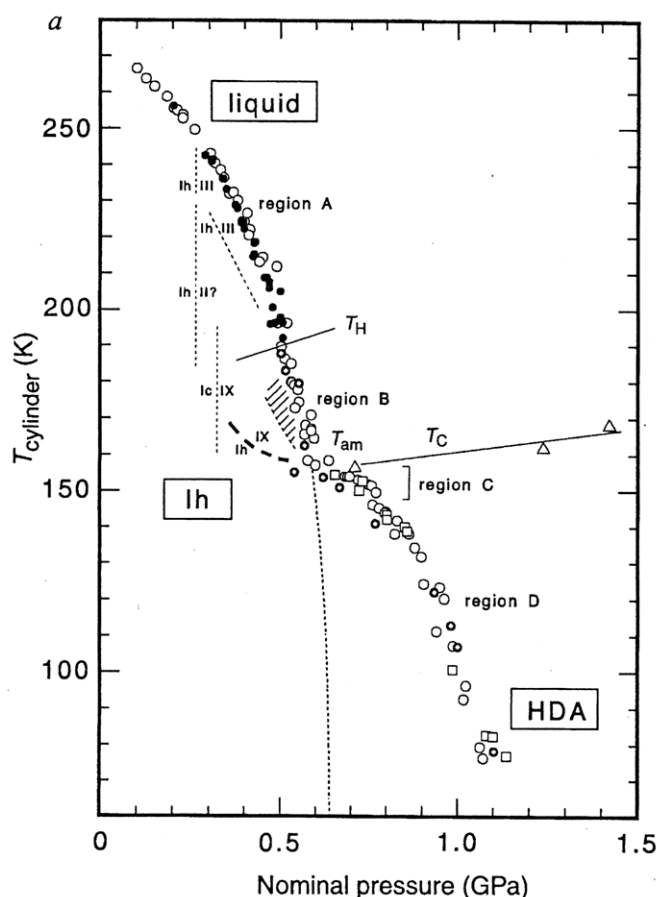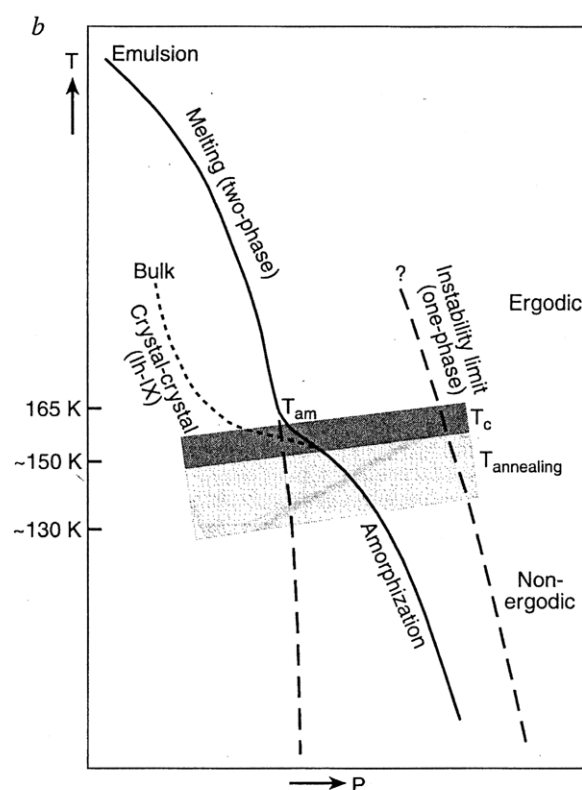
FIG. 2 a, The pressure-induced melting–amorphization line of ice Ih. Transition pressures were obtained by detecting a decrease in sample volume (empty circles, Ih emulsion; empty squares, pure bulk Ih) or a decrease (filled circles) or an increase (two concentric circles) in the sample temperature. When compression and decompression were repeated, crystal–crystal transitions (thin dotted lines) also occurred. They were distinguished from the melting transitions by their transition pressures, except near 245 K, 0.27 GPa and 200 K, 0.5 GPa. Around 200 K and 0.5 GPa, the Ih–III transition was exothermic, and the endothermic nature of the melting process revealed the onset melting pressure. The thick dotted line is the extrapolated thermodynamic melting line. The crystallization temperature of HDA (triangles and the T_c line) and the extrapolated homogeneous freezing temperature of supercooled water (the T_H line), are also shown. The hatched area corresponds to the gradual transition a in Fig. 1. The thick dashed line shows the ice Ih–IX transitions of pure bulk ice Ih. The melting line and the amorphization line merge around T_{am}. b, Schematic representation of the crossover from two-phase towards one-phase disordering.

In regions C ($\sim$160 K > T > $\sim$150 K) and D (below $\sim$150 K), I obtained the same results both for ice emulsions and for bulk ice Ih. In region C, I observed amorphization to high-density amorphous (HDA) ice followed by crystallization to ice IX. Above $\sim$160 K, bulk ice Ih is transformed to IX directly before melting (bold dashed line in Fig. 2a); so we can consider that in region C the HDA ice appears as an intermediate phase in this crystal–crystal transformation. The samples underwent 'over-pressurization' (Fig. 1, region C)—a transformation beginning at point c lowered the pressure to point d. The emulsion sample recovered at 1 bar from point c showed two exothermic transitions on heating—first to low-density amorphous (LDA) ice and then to crystalline ice Ic[1,6]. The location of the first transition is consistent with its identification with the HDA → LDA transition, showing that HDA ice is present in the sample at c—although the X-ray diffraction pattern showed only untransformed ice Ih, the HDA halo being presumably too weak to detect. The sample from d showed the X-ray pattern of ice IX, and I suppose that the exothermic amorphization at c induces this crystallization.

Although the slope of the melting/amorphization curve changes rather abruptly from region B to C, I believe that the crossover here is continuous. Primarily this is because the shape of the compression curve of melting at b in region B below about 165 K is the same as that of amorphization in region C, with a slight over-pressurization and subsequent pressure relaxation. I therefore suggest that the melting transition in region B changes smoothly to amorphization (followed by crystallization) at a temperature T_{am} between 165 and 155 K in region C (Fig. 2b).

In region D, amorphization of ice Ih to HDA occurred without any subsequent crystallization—all recovered samples were identified as HDA by X-ray and thermal analysis. Thus, ice Ih melts in region A, melts and freezes in region B, amorphizes and crystallizes in region C and amorphizes in region D, with a continuous crossover between these behaviours.

Although all samples recovered from region D were HDA ice, their X-ray patterns and HDA–LDA transition temperatures varies slightly with amorphization temperature (Fig. 4). HDA ice formed by amorphization at 77 K and heated to $\sim$140 K at 1.5 GPa resembled that obtained by amorphization at 140 K. Moreover, the HDA ices made by transformation not only of ice Ih[1] but also ice Ic[7] and LDA ice[8,9] under various pressure–temperature conditions all show identical X-ray patterns (with a halo peak around 2.75 Å) and similar HDA–LDA transition temperatures (around 123–128 K) when heated or annealed to 130–150 K at 1.0–1.5 GPa. This shows that the different HDA ices are all in the same HDA 'megabasin' on the potential-energy surface[10]—that is, they are different metastable states that can be annealed to the same (relaxed) HDA potential minimum.
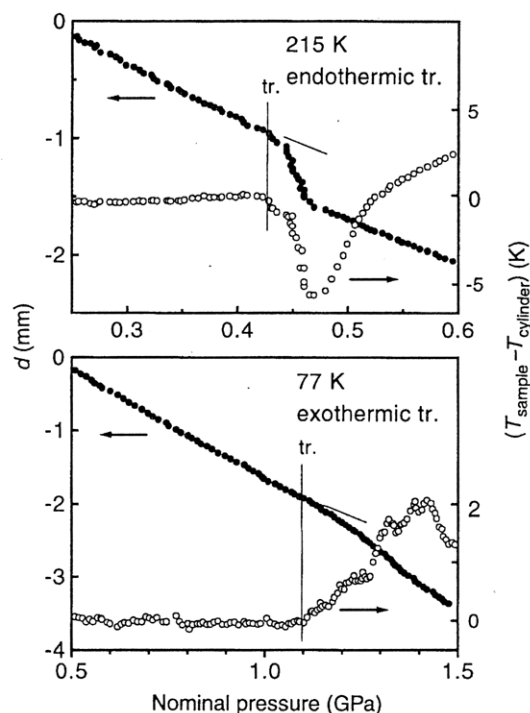
FIG. 3 Piston displacement d, and difference in temperature between the sample and the cylinder, during compression of ice Ih emulsions. Data were obtained at 215 K (top panel) and 77 K (bottom panel). The sample temperature was measured during compression (and during heating at a constant nominal pressure) by a thermocouple brought into the sample through a small hole in a piston[9]. When steadily heated, the sample temperature was lower than the cylinder temperature by ~4 K at ~140 K, ~2.5 K at ~160 K, and ~1 K at ~200 K. The transition (tr.) pressure was defined as the pressure at which the volume started to decrease where the sample temperature clearly began to change.

I performed differential thermal analysis (DTA) of preheated or annealed pure HDA ice at high pressures to determine the glass transition temperature T_g of the relaxed HDA ice—that is, the temperature at which the molecular motion of supercooled water 'freezes out' to form the glassy HDA phase. I observed pressure-dependent crystallization of HDA ice (an exothermic transition) at temperatures shown as T_c in Fig. 2, and the line of transition temperatures apparently crosses the melting/amorphization curve around T_{am}, which is consistent with the idea that amorphization occurs only below T_{am}, and melting followed by crystallization above it. But the DTA experiments showed no signature of an endothermic glass transition (to within $\pm$ ~0.02 K) before crystallization, implying that either T_g is very close to T_c or the difference in heat capacity between HDA and supercooled water is too small to be detected. Nevertheless, the glass transition temperature should be above, or near, the temperature at which HDA ice can be annealed from metastable forms (that is, 130–150 K) and is usually below T_c (155–160 K), so I propose that it lies in the region 150–160 K at 0.6–0.8 GPa. This value is close to the ideal glass transition temperature derived for supercooled water at high pressure by fitting diffusion data to the Vogel–Tammann–Fulcher equation[11].

As the temperature decreases below T_{am}, the amorphization line bends such that amorphization goes from being more temperature-sensitive (between 160 and 140 K) to more pressure-sensitive (below ~140 K). This suggests that at higher pressures the potential barrier for amorphization decreases and some kind of mechanical instability of ice Ih is being approached[4]. In other words, the amorphization mechanism may change gradually from being a kind of kinetically delayed 'melting' (a two-phase picture) towards a collapse due to lattice instability (a one-phase picture). Thus, in region C we might suppose that the motion of water
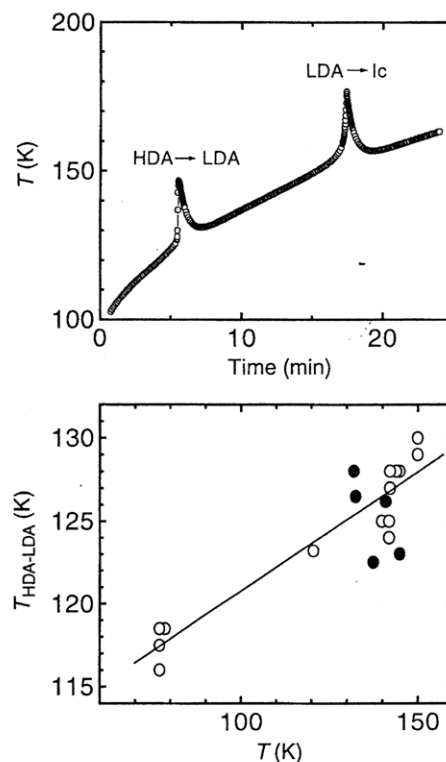

FIG. 4 Top panel, a typical heating curve of high-density amorphous (HDA) ice at 1 bar (LDA, low-density amorphous ice; Ic, ice Ic). Bottom panel, HDA–LDA transition temperatures of HDA ices. Open circles, HDA formed by amorphization at T K; filled circles, HDA heated (or annealed) to T K under high pressure. Sample grains (~150 mg) were loaded in a thin aluminium cup (~15 mg) placed inside a steel pipe which was heated from 77 K to room temperature (at a rate of about 2–4 K min^{-1} around 120–160 K). The temperature of the cup was measured with an attached fine thermocouple. The HDA showed two exothermic transitions[1,6], whereas ice IX showed an exothermic transition to ice Ic[16,17] at ~155 K. The samples were also studied by X-ray diffraction; a glass vacuum flask[9] having a capillary for X-ray diffraction was used. X-ray photographs of sample fragments (0.2–0.5 mm in size) in the flask filled with liquid nitrogen were taken using Zr-filtered Mo radiation and Polaroid films. Crystalline phases were determined by their 'ring' patterns, which occurred on a background 'halo' derived from the glass capillary, the liquid nitrogen and the emulsion carrier materials. HDA and LDA were differentiated by the position and width of their principle diffraction halo rings[1,8,9]. The HDA formed by amorphization at 145 K had an intense halo ring corresponding to an interplanar spacing of ~2.75 Å; this peak was absent from the X-ray pattern of HDA formed by amorphization at 77 K.

molecules becomes too slow for melting (at the extrapolated, thick short-dashed line in Fig. 2a) to take place on experimental timescales, so that the ice Ih can be 'supercompressed'. This is supported by my supposition that the glass transition ('freezing' of motion in supercooled water) occurs around T_{am}. So in region C and down to around 140 K we can regard the transformation of ice Ih as a supercompression followed by 'melting' to a highly viscous liquid, or alternatively, by amorphization to a nearly relaxed HDA ice. Either way, amorphization is clearly not a matter of melting to an equilibrium liquid followed by arrest of molecular motion; rather, it is a transition to an unrelaxed amorphous state which then slowly relaxes further towards a more stable glass-like state. (Below ~140 K this relaxation becomes slow on experimental timescales and the HDA ice remains to all intents and purposes unrelaxed). The corollary is that the liquid state (above T_{am}), the viscous liquid or relaxed amorphous state between ~160 and ~140 K, and the unrelaxed HDA states below ~140 K all lie within the same HDA megabasin in configuration space. How this relates to other kinds of amorphization[12-15] remains an open question at this stage. □

1. Mishima, O., Calvert, L. D. & Whalley, E. *Nature* **310**, 393–395 (1984).
2. Wolf, G. H. *et al.* in *High-Pressure Research: Application to Earth and Planetary Sciences* (eds Syono, Y. & Manghnani, M. H.) 503–517 (Terra Science, Tokyo/Am. Geophys. Union, Washington DC, 1992).
3. Tse, J. S. & Klein, M. L. *J. Chem. Phys.* **92**, 3992–3994 (1990).
4. Sciortino, F. *et al. Phys. Rev. E* **52**, 6484–6491 (1995).
5. Kanno, H., Speedy, R. J. & Angell, C. A. *Science* **189**, 880–881 (1975).
6. Handa, Y. P., Mishima, O. & Whalley, E. *J. Chem. Phys.* **84**, 2766–2770 (1986).
7. Johari, G. P., Hallbrucker, A. & Mayer, E. *J. Phys. Chem.* **94**, 1212–1214 (1990).
8. Mishima, O., Calvert, L. D. & Whalley, E. *Nature* **314**, 76–78 (1985).
9. Mishima, O. *J. Chem. Phys.* **100**, 5910–5912 (1994).
10. Angell, C. A. *Science* **267**, 1924–1935 (1995).
11. Lüdemann, H.-D. *Ber. Bunsenges. Phys. Chem.* **94**, 325–332 (1990).
12. Johnson, W. L. *Prog. Mater. Sci.* **30**, 81–134 (1986).
13. Cahn, R. W. & Johnson, W. L. *J. Mater. Res.* **1**, 724–732 (1986).
14. Wolf, D., Okamoto, P. R., Yip, S., Lutsko, J. F. & Kluge, M. *J. Mater. Res.* **5**, 286–301 (1990).
15. Fecht, H. J. *Mater. Trans. Jpn Inst. Metals* **36**, 777–793 (1995).
16. Bertie, J. E., Calvert, L. D. & Whalley, E. *J. Chem. Phys.* **38**, 840–846 (1963).
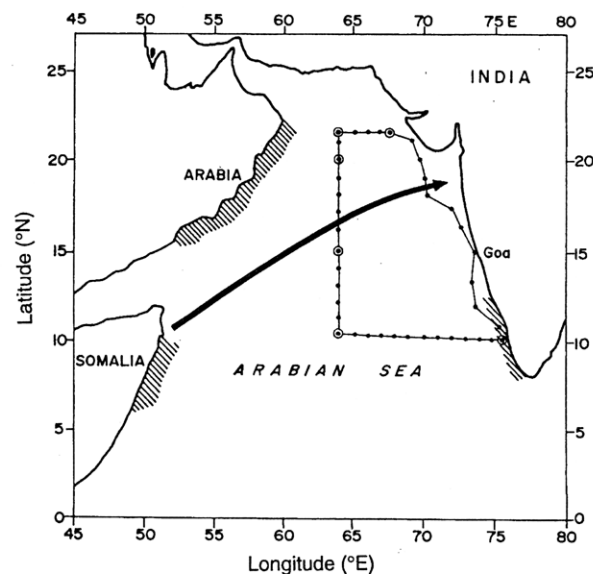17. Handa, Y. P., Klug, D. D. & Whalley, E. *Can. J. Chem.* **66**, 919–924 (1988).

FIG. 1 Cruise track in the Arabian Sea; open circles denote positions where biological data were collected. Temperature, salinity and nutrient profiles were collected from stations shown by both open and filled circles. Hatched areas show regions where coastal upwelling takes place along Somalia, Arabia and the southwestern coast of India during the summer monsoon. The axis of the Findlater Jet, active during this season, is shown by the arrow; northwest of this axis, open ocean upwelling takes place due to positive wind-stress curl and upward Ekman pumping. Temperature, salinity and nutrient profiles were taken at one degree intervals using a Sea-Bird CTD system. Nutrients were analysed with a SKALAR auto-analyser. Primary productivity was measured following ^{14}C clean *in situ* method, chlorophyll a was determined with a fluorometer and phytoplankton cells (>5 μm) were enumerated with an inverted microscope. Zooplankton in the upper mixed layer were collected during the night with a 200-μm mesh; microzooplankton were collected by filtering 20 litres water through a 20-μm mesh. Bacteria and picoplankton were counted using epifluorescence microscopy.
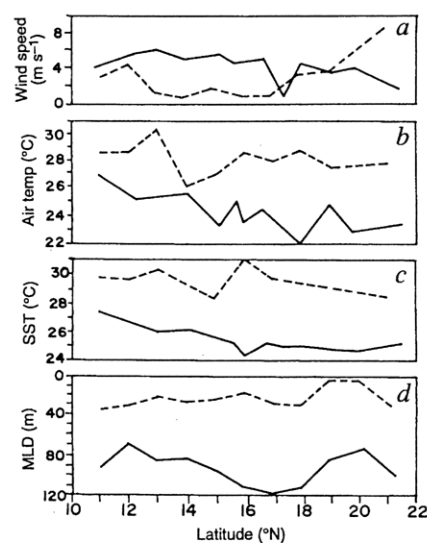
Mechanism of the biological response to winter cooling in the northeastern Arabian Sea

M. Madhupratap*, S. Prasanna Kumar*,
P. M. A. Bhattathiri*, M. Dileep Kumar*,
S. Raghukumar*, K. K. C. Nair† & N. Ramaiah*

* National Institute of Oceanography, Dona Paula, Goa 403 004, India
† Regional Centre of NIO, Cochin 682018, India

THE Arabian Sea is one of the most biologically productive ocean regions[1], mainly due to the upwelling of nutrients during the summer (southwest) monsoon. But the northern Arabian Sea continues to sustain fairly high biological production after the upwelling season and during much of the winter (northeast) monsoon[2–4]. The processes that enable this high winter productivity have hitherto been poorly understood, being variously attributed to surface cooling effects[2,3] or wind-driven changes in ocean circulation[4]. Here we present physical, chemical and biological data that indicate that sea surface cooling drives convection processes that lead to the injection of nutrients up into the surface waters of the northeastern Arabian Sea during winter, and that this mechanism of nutrient supply is a dominant control on winter productivity. Observed seasonal changes in bacterial and microzooplankton populations may provide an explanation for the Arabian Sea 'paradox'[5–8] that mesozooplankton biomass remains more or less invariable throughout the year.

Data were collected in two Joint Global Ocean Flux Study (JGOFS) cruises of ORV *Sagar Kanya* (Fig. 1); 12 April–12 May 1994 (inter-monsoon) and 3 February–5 March 1995 (winter). The physical and chemical conditions during these two cruises were distinctly different. During February 1995, winds were predominantly north/north-easterlies (average speed ~4 m s^{-1}) along 64° E. Sea surface temperature (SST) was 27.5 °C at 11° N and decreased at a rate of about 0.5 °C per degree latitude up to 16° N (Fig. 2). Similarly, air temperature dropped from 26.5 °C in the south to <24 °C in the north. The most dramatic change was observed in the mixed-layer depth (MLD) which was thick between 15° and 18° N with a maximum of 120 m at 15° N, but thinned steadily towards the south to 65 m. The salinity structure also showed a deep isohaline layer (100 m thick with >36.4 practical salinity units, psu) in the north which became thinner

FIG. 2 North-south variations (along 64° E) in wind speed (*a*), air temperature (*b*), sea surface temperature (SST; *c*), and mixed layer depth (MLD; *d*) during winter (solid line) and the inter-monsoon period (broken line). Measurement uncertainties are ±0.1 ms^{-1}, ±0.5 °C, ±0.5 °C and ±1 m, respectively. The MLD was defined as the depth where the sea temperature was 1 °C less than the SST value.